Magnetic Field Alignment in Galaxy Simulations

Mariya Bizunova

Division of Astrophysics
Department of Physics

LUND UNIVERSITY

2026-EXA256 FYSK04

Bachelor′s degree project of 15 higher education credits
May 2026

Supervisor: Raghav Arora

Division of Astrophysics
Department of Physics
Box 118
SE-221 00 Lund
Sweden

Abstract

Spiral galaxies host elongated filamentary structures of dense gas and dust, known as feathers, which branch off the main spiral arms into the interarm regions and are associated with star formation. The physical mechanisms governing their formation remain debated, with magnetic fields proposed as one of the contributing factors. This thesis investigates the role of magnetic fields in feather formation by analysing isolated galaxy simulations of self-gravitating, isothermal, magnetised discs. Two simulation runs are compared, differing only in the strength of the initial toroidal magnetic field: a strongly magnetised case at equipartition ($\beta = 1$) and a weakly magnetised case at sub-equipartition ($\beta = 10$). The geometric relationship between the gas structures and the local magnetic field is quantified using the Histogram of Relative Orientations (HRO), which gives a statistical measure of the alignment between the gas structures and the magnetic field as a function of log-normalised projected surface density.

The simulations reveal that in the strongly magnetised regime, the transition from parallel to perpendicular alignment between the gas structures and the magnetic field begins already at lower densities, well before the feather formation threshold is reached. In the weakly magnetised regime, this transition occurs much later, close to the feather formation threshold itself. Beyond this threshold, both regimes converge to predominantly perpendicular alignment, with the dense feather structures forming preferentially across the field lines rather than along them. However, the strongly magnetised case reaches a more negative value of the alignment parameter, indicating that this configuration is more dominant when the magnetic field is dynamically important. These results suggest that the density at which the alignment transition occurs may serve as an observational indicator of the dynamical importance of the magnetic field in galactic discs.

Magnetic Fields and the Feathers of Galaxies

When you look at a photograph of a spiral galaxy, your eyes are immediately drawn to the bright, swirling arms made of billions of glowing stars. However, what we can see is only half the story. The space between these stars is not empty, it is filled with a vast ocean of gas and dust. If you look closely with a powerful telescope, you will see smaller, delicate wisps of gas branching off the spiral arms and reaching into the regions between them. Astronomers call these structures 'feathers'. These galactic feathers are far more than just cosmic decorations. They are among the cold, dense lanes of gas in a galaxy, and they are exactly the kind of place where gravity can pull matter together tightly enough to give birth to new stars.

But how do these feathers form in the first place? While astrophysicists are still debating the exact causes, one of the prime suspects is something completely invisible to the human eye: magnetic fields. Just as the Earth has a magnetic field that causes compass needles to point north, entire galaxies have their own enormous magnetic fields threading through them. You can think of galactic magnetic fields as giant, invisible elastic bands weaving through the swirling gas. In my thesis, I set out to understand the relationship between these invisible bands and the dense gas feathers where stars are born.

Because it takes tens of millions of years for a real galaxy to evolve, we cannot simply watch one through a telescope to see what happens. Instead, astrophysicists use powerful computers to build a galaxy in a box. By programming the laws of physics into a simulation, they can hit fast-forward and watch how the gas, gravity, and magnetic fields interact over time. For my thesis, I worked with two such simulations that differed only in one aspect: the strength of the magnetic field threading through the gas. My job was to analyse them and figure out how magnetic fields change the way feathers are formed.

What the simulations reveal is a clear shift in how the gas and magnetic fields are arranged at different densities. In the less crowded parts of the galaxy, the gas structures tend to lie along the magnetic field. As gravity gathers more and more gas into one place, this neat parallel arrangement starts to break down. The reason has to do with the shape of the structures that gravity builds. Feathers are long and narrow, stretching outward from the galactic center, while the magnetic field winds around the galaxy in circles. The two directions naturally cross, so the feathers end up lying across the field rather than along it. This crossing pattern appears whether the magnetic field is strong or weak, but it is sharper and more pronounced when the field is strong.

This crossing pattern is useful for astronomers: it tells us something about the role magnetic fields play in shaping the feathers. By studying this interplay between gravity and magnetic fields, we can better understand how these giant feathers in the sky formed, and potentially where the next generation of stars will be born.

Contents

1 Introduction

1.1 Magnetic Fields in Galaxies

The space between stars in a galaxy is filled with gas and dust, together known as the interstellar medium (ISM). The ISM is permeated by magnetic fields, which exert forces on the gas and affect its dynamics. Although weak compared to laboratory fields, magnetic fields are dynamically important in galaxies and are relevant to many astrophysical processes, including star formation and the propagation of cosmic rays (Han, 2017).

Magnetic fields in galaxies cannot be measured directly and are quantified from their effects on observed radiation (Han, 2017). Several complementary methods are used, each sensitive to a different phase of the ISM. Radio synchrotron emission is produced by relativistic electrons spiraling along magnetic field lines and traces the field in the warm, diffuse gas. Polarised thermal emission from magnetically aligned dust grains, observed at far-infrared wavelengths, traces the field in the colder and denser regions of the disc (Borlaff et al., 2023). Together, these observations show that galactic magnetic fields are ordered on kiloparsec scales and follow the spiral structure of the disc (Beck, 2016).

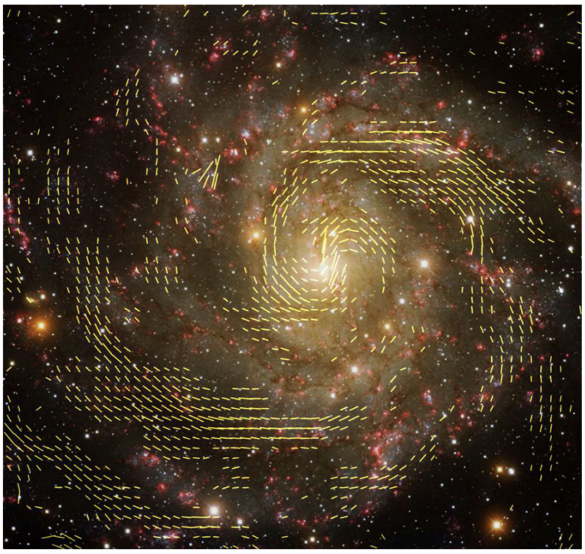

Figure 1: Magnetic field orientation in the spiral galaxy IC 342. The overlaid vectors represent the large-scale, ordered magnetic field derived from polarised radio observations. Figure adopted from Beck (2016), combining radio data with an optical colour image from the Kitt Peak Observatory. Copyright: MPIfR Bonn.

An example is shown in Figure 1 for the nearby spiral galaxy IC 342. The vectors, derived from polarised radio observations, trace the orientation of the ordered magnetic field and follow the visible spiral arms across the disc. A similar correspondence between magnetic field and spiral morphology is observed in many spiral galaxies and indicates that the field is coupled to the gas of the ISM (Beck, 2016).

1.2 Dense Gas Structures and Feathers

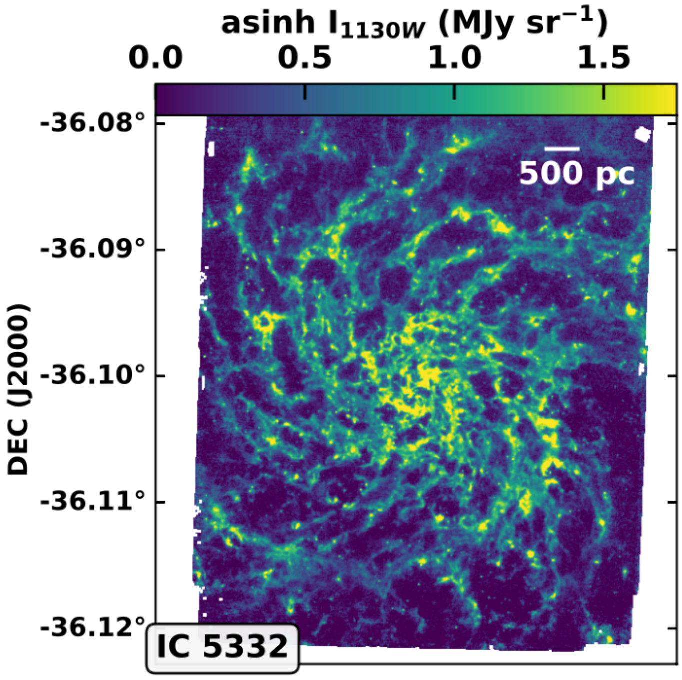

Figure 2: High-resolution observation revealing the network of dense dust filaments (feathers) in the disc galaxy IC 5332. Taken with the James Webb Space Telescope (JWST), this image demonstrates the elongated substructures extending outward from the main spiral arms into the interarm regions. Image adapted from Meidt et al. (2023).

Observations of nearby star-forming disc galaxies reveal elongated filamentary structures of gas and dust that branch off the main spiral arms and extend into the regions between them. These features are commonly referred to as feathers and were described in detail by La Vigne et al. (2006) in a survey of spiral galaxies, observed with the Hubble Space Telescope.

Feathers are astrophysically significant because they represent sites of dense molecular gas accumulation and are potentially associated with ongoing star formation. More recent infrared observations with the James Webb Space Telescope (JWST) offer significantly higher resolution, demonstrating more detailed morphology of these structures. Figure 2 shows an example for the disc galaxy IC 5332, where the interstellar medium appears organised into a network of filamentary structures extending across kiloparsec scales (Meidt et al., 2023). Similar networks have been reported in several other nearby galaxies, suggesting that feathers may be a common component of star-forming discs (Meidt et al., 2023).

Feathers are generally understood to form through gravitational instability within the cold gas of the disc. However, the mechanism of their formation, and the extent to which physical processes such as gravitational instability, magnetic fields etc. play a role is still debated.

1.3 The Role of Magnetic Fields in Feather Formation

The role of self-gravity alone in feather formation was investigated by Arora et al. (2025), who showed through isothermal hydrodynamical simulations that gravitational instability combined with differential rotation is sufficient to produce feather structures, without invoking magnetic fields, stellar feedback, or any other external processes.

In real galaxies, however, the ISM is subject to various additional physical processes that may also influence the formation of dense gas structures. These include, for example, supernova feedback from massive young stars (Kim et al., 2020) and the Parker instability (Körtgen et al., 2019). Among the proposed mechanisms, magnetic fields have received particular attention. Numerical simulations of strongly magnetized, self-gravitating galactic discs have shown that the Parker instability can drive the formation of giant filamentary regions in the disc, which subsequently become gravitationally unstable and fragment into dense concentrations of gas (Körtgen et al., 2019). Magnetic fields are therefore known to play a potential role in feather formation, but the extent to which they influence this process has not been fully established.

This thesis builds directly on the framework of Arora et al. (2025) by extending the analysis to magnetohydrodynamics simulations in which a toroidal magnetic field is included from the outset. By comparing simulation runs at two different field strengths, a weakly magnetized and a strongly magnetized case, it becomes possible to isolate how the inclusion of a magnetic field affects the resulting gas structures and their orientation relative to the local field direction.

To quantify this alignment, the HRO method is applied (Soler & Hennebelle, 2017). The method was originally introduced by Soler et al. (2013) to study the relative orientation between the magnetic field and the gas density structures in molecular clouds, which are far smaller than entire galactic discs. An example is shown in Figure 3, where the orientation of the magnetic field is overlaid on the gas density of a simulated molecular cloud; the relative orientation changes from parallel to the field in the low-density gas to perpendicular in the dense regions, when the magnetic field is dynamically important. A distinguishing feature of this thesis is the application of the same technique on the much larger galactic scale, in contrast to the molecular-cloud scales on which it was used. This technique measures the statistical orientation of gas density structures relative to the local magnetic field vector as a function of gas density, making it possible to track how the geometric relationship between the gas and the field evolves from the diffuse interarm gas through to the fully formed feather structures. Applying the HRO method to the two cases allows us to investigate whether the formation process leaves an imprint in this alignment that may be used to quantify the influence of the magnetic field. In the future, the same approach could potentially be applied to observational data. The central question this thesis addresses is therefore: *How does the alignment between the gas density and the magnetic field evolve from the diffuse ISM down to the dense, feather-formed regions under varying levels of magnetization?*

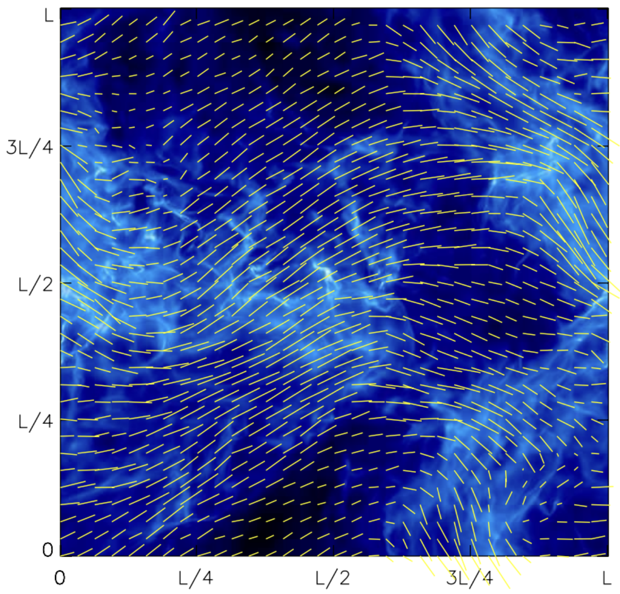

Figure 3: Relative orientation between the magnetic field and the gas density structures in a simulated molecular cloud. The coloured map shows the gas density and the overlaid segments indicate the local magnetic field orientation. The alignment between the density structures and the field changes from parallel in the low-density gas to perpendicular in the densest regions. Figure adapted from Soler et al. (2013).

The thesis is structured as follows. Section 2 presents the theoretical framework, covering the equations of ideal MHD, the definition of the alignment angle, and the HRO method. Section 3 describes the simulation setup and analysis methodology. Section 4 presents the results, covering the disc morphology, magnetic field topology, global alignment maps, and the density-dependent HRO analysis. Section 5 discusses the physical interpretation of the results and prospects for observational comparison.

2 Theoretical Framework

2.1 Ideal Magnetohydrodynamics (MHD)

In galactic simulations, the gas in the interstellar medium is modeled as a magnetized, compressible fluid. The dynamic evolution of the gas is governed by the equations of ideal magnetohydrodynamics (MHD). The framework relies on several key physical assumptions: the plasma is strictly quasi-neutral, non-relativistic, inviscid (lacking internal viscosity), and can be treated as a single continuous fluid (Choudhuri, 1998). As shown below, each of these assumptions is behind the derivation of the governing equations.

The first governing equation expresses the conservation of mass. Since the gas is neither created nor destroyed, the mass contained in any fixed volume can change only through a net flux of gas across its surface. This balance is expressed by the continuity equation:

$$\frac{\partial \rho}{\partial t} + \nabla \cdot (\rho \mathbf{v}) = 0, \tag{1}$$

where ρ is the gas density and $\mathbf{v}$ is the velocity field.

The motion of the gas is obtained from Newton's second law applied to the fluid. Because the gas is assumed to be inviscid, the starting point is the Euler equation. For a fluid subject to a thermal pressure P and a gravitational potential Φ:

$$\rho\left(\frac{\partial \mathbf{v}}{\partial t}+(\mathbf{v}\cdot\nabla)\mathbf{v}\right)=-\nabla P-\rho\nabla\Phi. \tag{2}$$

In a plasma, the gas carries currents and therefore experiences an additional Lorentz force. The general electromagnetic force per unit volume is $\rho_q\mathbf{E}+\frac{1}{c}\mathbf{j}\times\mathbf{B}$, where ρ_q is the charge density and $\mathbf{j}$ the current density. The assumption of quasi-neutrality ($\rho_q \approx 0$) removes the electric contribution, leaving the magnetic body force:

$$\mathbf{f}_L=\frac{1}{c}\mathbf{j}\times\mathbf{B}. \tag{3}$$

The current density is related to the magnetic field through Ampère's law. In the non-relativistic limit the displacement current is of order v^2/c^2 and is neglected, so we get:

$$\mathbf{j}=\frac{c}{4\pi}\nabla\times\mathbf{B}. \tag{4}$$

Substituting Eq. (4) into Eq. (3) and adding the resulting force to the right-hand side of Eq. (2) yields the MHD momentum equation:

$$\rho\left(\frac{\partial \mathbf{v}}{\partial t}+(\mathbf{v}\cdot\nabla)\mathbf{v}\right)=-\nabla P-\rho\nabla\Phi+\frac{1}{4\pi}(\nabla\times\mathbf{B})\times\mathbf{B}. \tag{5}$$

When the final term is expanded using the vector identity $(\nabla\times\mathbf{B})\times\mathbf{B}=(\mathbf{B}\cdot\nabla)\mathbf{B}-\frac{1}{2}\nabla B^2$, that gives:

$$\frac{1}{4\pi}(\nabla\times\mathbf{B})\times\mathbf{B}=\underbrace{\frac{1}{4\pi}(\mathbf{B}\cdot\nabla)\mathbf{B}}_{\text{magnetic tension}}-\underbrace{\nabla\left(\frac{B^2}{8\pi}\right)}_{\text{magnetic pressure}}. \tag{6}$$

The second term has the form of a pressure gradient with magnetic pressure $P_{\mathrm{mag}}=B^2/8\pi$, which resists compression of the field, while the first term represents a tension along the field lines that resists their bending.

The final equation governs the evolution of the magnetic field itself and follows from combining Faraday's law with Ohm's law for the conducting fluid. Faraday's law relates the time variation of the magnetic field to the electric field:

$$\frac{\partial \mathbf{B}}{\partial t}=-c\nabla\times\mathbf{E}. \tag{7}$$

For a fluid moving with velocity $\mathbf{v}$, the current is driven by the electric field measured in the local rest frame of the gas, giving Ohm's law:

$$\mathbf{j}=\sigma\left(\mathbf{E}+\frac{1}{c}\mathbf{v}\times\mathbf{B}\right), \tag{8}$$

where σ is the electrical conductivity. Solving Eq. (8) for $\mathbf{E}$ and substituting the current from Eq. (4) shows:

$$\mathbf{E}=\frac{c}{4\pi\sigma}\nabla\times\mathbf{B}-\frac{1}{c}\mathbf{v}\times\mathbf{B}. \tag{9}$$

Inserting this expression into Faraday's law, Eq. (7), and using the identity $\nabla\times(\nabla\times\mathbf{B})=-\nabla^2\mathbf{B}$, which follows from the solenoidal condition $\nabla\cdot\mathbf{B}=0$, gives the induction equation:

$$\frac{\partial \mathbf{B}}{\partial t}=\nabla\times(\mathbf{v}\times\mathbf{B})+\eta\nabla^2\mathbf{B},\qquad \eta\equiv\frac{c^2}{4\pi\sigma}. \tag{10}$$

The first term on the right-hand side describes the advection of the magnetic field by the gas flow, while the second describes its resistive diffusion through the gas, with η the magnetic diffusivity. The relative importance of these two is quantified using the magnetic Reynolds number defined here:

$$R_m = \frac{|\nabla \times (\mathbf{v} \times \mathbf{B})|}{|\eta \, \nabla^2 \mathbf{B}|} \sim \frac{VL}{\eta}, \tag{11}$$

where V and L are the characteristic velocity and length scales of the system. Considering very large length scales involved, galactic discs are characterised by $R_m \gg 1$ (Ferrière, 2020), so that the diffusion term is negligible compared to the advection term. This corresponds to the limit of infinite conductivity ($\sigma \to \infty$, $\eta \to 0$), which defines the ideal MHD approximation. In this limit the induction equation reduces to:

$$\frac{\partial \mathbf{B}}{\partial t} = \nabla \times (\mathbf{v} \times \mathbf{B}). \tag{12}$$

This equation establishes the theorem of flux freezing. Magnetic flux is defined as the total amount of magnetic field passing through a given surface area of the fluid, which remains constant. This dictates that the magnetic field lines are perfectly coupled to the fluid itself. Consequently, when the gas flows perpendicular to the magnetic field, the field lines are passively dragged and deformed alongside the moving fluid (see Figure 4).

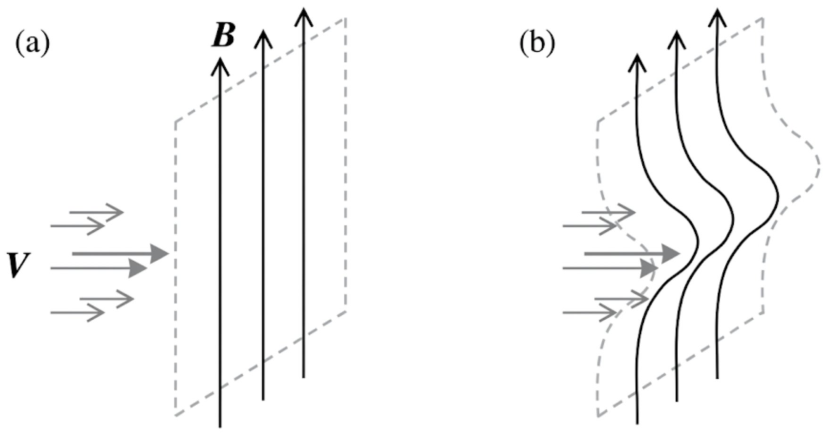

Figure 4: Illustration of magnetic flux-freezing. (a) An initially uniform magnetic field passing through a horizontal shear flow. (b) The resulting distortion of the magnetic field lines, which are passively dragged and deformed by the moving fluid. Adapted from Shukurov & Subramanian (2021).

2.2 The Magnetic Alignment Angle

To quantitatively analyze the geometric relationship between the galactic gas structures and the local magnetic field, we measure the relative orientation angle $\cos\phi$. The relative angle between the local density gradient ($\nabla\rho$) and the local magnetic field vector ($\mathbf{B}$) is calculated using the dot product:

$$\cos\phi = \frac{\nabla\rho \cdot \mathbf{B}}{|\nabla\rho||\mathbf{B}|} \tag{13}$$

Because feathers possess an elongated filamentary geometry and act as local density maxima, their physical elongation is inherently perpendicular to the direction of the steepest density increase. Therefore, the local density gradient ($\nabla\rho$) serves as a normal vector to the feather's surface. Because of this geometric relationship, the orientation angle between $\nabla\rho$ and $\mathbf{B}$ directly reflects the orientation of the structure itself relative to the field, as illustrated in Figure 5.

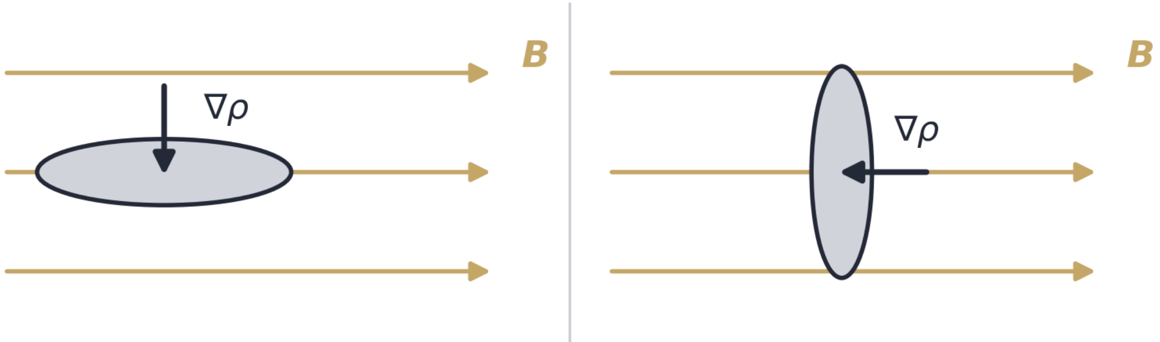

Figure 5: Schematic illustration of the relative orientation between a gas structure and the local magnetic field $\mathbf{B}$, where the density gradient $\nabla\rho$ points perpendicular to the elongation of the structure. (Left) A structure elongated along the field lines, so that $\nabla\rho$ is perpendicular to $\mathbf{B}$ and $\cos\phi \approx 0$, corresponding to parallel alignment. (Right) A structure elongated across the field lines, so that $\nabla\rho$ is parallel to $\mathbf{B}$ and $\cos\phi \approx \pm 1$, corresponding to perpendicular alignment.

Evaluating $\cos\phi$ provides a direct geometric interpretation of the gas alignment. A value of $\cos\phi \approx 0$ indicates that the density gradient is orthogonal to the magnetic field, meaning the physical feather structure is aligned parallel to the field lines. Conversely, values approaching $\cos\phi \approx \pm 1$ indicate that the gradient is parallel or anti-parallel to the magnetic field, signifying that the feather structure is oriented perpendicular to the field lines. The use of the absolute value $|\cos\phi|$ in the subsequent analysis reflects the fact that it is the alignment of the structure relative to the field that is of physical interest, rather than the direction along the field in which the gradient points. A field pointing parallel or anti-parallel to a given density gradient describes the same physical alignment, and the two cases are therefore treated equivalently.

2.3 Histogram of Relative Orientations (HRO)

To get a statistical measure for the alignment of magnetic fields with feathers throughout the galaxy, we use the HRO. Rather than considering the orientation angle at a single location, the HRO collects the relative orientations measured across many points and represents their statistical distribution as a histogram of $|\cos\phi|$. The histogram is evaluated using the dimensionless shape parameter ζ, defined as:

$$\zeta = \frac{A_c - A_e}{A_c + A_e} \tag{14}$$

A_c and A_e represent the integrated area under the regions defined by $0 < |\cos\phi| < 0.25$ and $0.75 < |\cos\phi| < 1.00$ respectively. These are the central regions and the regions at the extreme values of ϕ, as shown in Figure 6. The difference between these two areas is normalised by their sum, so that ζ is bounded between -1 and $+1$ and is independent of the total number of points sampled.

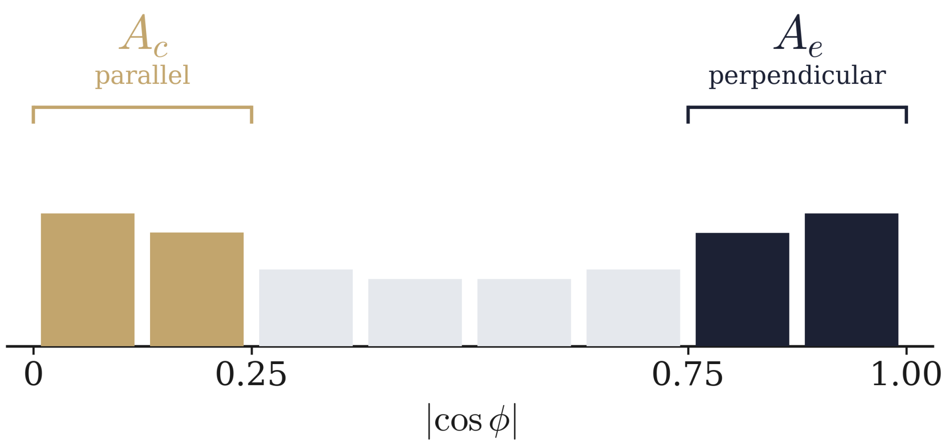

Figure 6: Schematic illustration of the HRO, showing the distribution of $|\cos\phi|$ values. The shape parameter ζ compares the integrated area A_c in the central region ($0 < |\cos\phi| < 0.25$), corresponding to parallel alignment, with the integrated area A_e in the extreme region ($0.75 < |\cos\phi| < 1.00$), corresponding to perpendicular alignment.

A positive value ($\zeta > 0$) indicates that the central area dominates, demonstrating that the galactic gas structures are predominantly parallel to the magnetic field. A negative value ($\zeta < 0$) indicates that the extreme areas dominate, establishing that the gas structures are aligned perpendicular to the magnetic field. A value approaching zero indicates a lack of coherent global alignment, corresponding to a flat histogram in which no orientation is preferred.

3 Methodology

3.1 Isolated Galaxy Simulations

Isolated galaxy simulations are used in this thesis. The simulated galaxies are modeled as three-dimensional, isothermal, and self-gravitating gaseous discs. For a detailed description, the reader is referred to Arora et al. (2025). At the beginning of the simulation ($t = 0$), the galactic disc is initialized in a state of hydrostatic equilibrium. The initial configuration ensures that the forces of thermal gas pressure balance the vertical pull of the gas's self-gravity towards the midplane. Simultaneously, in the radial direction, the outward centrifugal forces and thermal pressure gradients balance the inward gravitational forces to maintain a stable, rotating disc. The simulated disc is compact, extending to a radius of roughly 5 kpc, and is therefore smaller than large spiral galaxies such as the Milky Way. This reflects the idealised nature of the setup, in which the galaxy is characterised only by the dimensionless parameters Q and $\mathcal{M}_c$ rather than being scaled to reproduce a specific observed galaxy. The feather-forming region of interest lies at galactocentric radii of $R \approx 2$–4 kpc, which is the region on which the analysis and figures in this work are focused.

Building upon the hydrodynamical setup, the simulations analysed in this thesis additionally include a magnetic field. At $t = 0$, a toroidal magnetic field is initialized throughout the disc, uniformly aligned with the rotational flow of the gas. This configuration is chosen because the toroidal field is the dominant magnetic component observed in the disks of spiral galaxies. By analysing these magnetised runs, we can investigate how magnetic tension and magnetic pressure alter the overall morphology of the interstellar medium. To quantify this, a Plasma Beta (β) parameter is introduced and defined as the ratio of the gas thermal pressure ($P_{\rm th}$) to the magnetic pressure ($P_{\rm mag}$) as $\beta = \frac{P_{\rm th}}{P_{\rm mag}}$. Throughout this thesis, we specifically analyse two runs: a strongly magnetised case at equipartition ($\beta = 1$), where the magnetic pressure equals the thermal pressure, and a weakly magnetised case at sub-equipartition ($\beta = 10$), where the thermal pressure dominates by a factor of ten. That allows to directly compare the dynamics for both magnetised environments.

Following Toomre (1964), the global stability of the galactic disc is governed primarily by the Toomre Q parameter, defined as $Q = \frac{\kappa c_s}{\pi G \Sigma}$, where κ is the epicyclic frequency, c_s is the speed of sound, G is the gravitational constant, and Σ is the gas surface density. To trigger the fragmentation of the gas into filamentary feathers, the disc must be marginally unstable, requiring $Q \approx 1 - 2$. A disc with $Q \gg 1$ is gravitationally stable, since thermal pressure and rotational shear are strong enough to suppress density perturbations, whereas a disc with $Q \ll 1$ is strongly unstable and collapses rapidly without forming the filamentary structures of interest. Feather formation therefore requires the marginally unstable regime, in which self-gravity is just able to overcome the stabilising effects of pressure and rotation.

Furthermore, the structural evolution of the disc is controlled by the rotational Mach number ($\mathcal{M}_c$), defined as the ratio of the saturated circular velocity of the gas to the speed of sound ($\mathcal{M}_c = v_c/c_s$). This parameter dictates the relative amount of differential rotation and shear the gas undergoes, which alongside the Toomre Q parameter, governs the final morphology of the dense structures. A value of $\mathcal{M}_c = 29$ therefore describes a rotation-dominated disc in which the circular velocity is 29 times the sound speed, which is representative of the rotation speeds observed in nearby spiral galaxies. To ensure a consistent comparative analysis between the different magnetic regimes, this parameter is kept fixed at $\mathcal{M}_c = 29$ for all simulations in this work, so that any differences between the runs arise solely from the magnetic field strength.

Because the strength of the magnetic field affects how quickly the disc fragments, the two runs do not reach the onset of feather formation at the same physical time. As will be discussed in Section 4.1, the strongly magnetised disc ($\beta = 1$) fragments earlier, at $t = 39.97$ Myr, while the weakly magnetised disc ($\beta = 10$) reaches the equivalent stage only at $t = 59.97$ Myr. Throughout this work the two regimes are therefore compared at the onset of feather formation, that is, at the same evolutionary stage rather than at equal physical time. This ensures that the differences in the gas-field alignment reflect the influence of the magnetic field itself, rather than simply the fact that one run is more dynamically evolved than the other.

3.2 Histogram of Relative Orientations Analysis

To evaluate how the geometric relationship between the interstellar gas and the magnetic field evolves across the strongly and weakly magnetised environments, the spatial data is analyzed using the HRO technique. Building upon the theoretical framework established in Sections 2.3 and 2.2, the relative orientation angle $\cos\phi$ is computed numerically across the projected 2D simulation domain according to Eq. 13, using the local density gradient $\nabla\rho$ and the in-plane magnetic field vector $\mathbf{B}$. This calculation allows us to map the structural alignment of the gas across the entire disc.

The methodology is extended to investigate how magnetic alignment correlates with increasing gas density, rather than deriving a single global shape parameter for the entire galaxy. This density-dependent approach mirrors the analysis applied to turbulent magnetohydrodynamic environments, where the alignment parameter is evaluated as a function of particle density (Soler & Hennebelle, 2017). To achieve this, the projected surface density of the simulated disc is normalized by the initial central surface density (Σ_{c0}) and transformed into a logarithmic scale, $\log_{10}(\Sigma/\Sigma_{c0})$. A logarithmic scale is explicitly utilized to ensure a statistically balanced distribution of data points across the entire density range. The data is then partitioned into N number of uniformly spaced bins spanning the minimum to maximum limits of the logarithmic density.

The HRO shape parameter (ζ), as defined theoretically in Eq. (14), is computed independently for each bin. This is done by calculating the central (A_c) and extreme (A_e) areas of the local $\cos\phi$ probability density function strictly for the pixels that fall within that corresponding density range. Then a discrete ζ value is evaluated for each density interval, establishing the alignment parameter as a function of surface density. This density-dependent distribution directly maps the structural evolution of the gas: ζ values approaching $+1$ indicate that the physical structures are predominantly aligned parallel to the magnetic field, values near -1 establish a perpendicular structural alignment, and values around 0 reflect an inconclusive or random orientation. By plotting this distribution across the density bins, we can precisely trace the gas structures' transitions between parallel and perpendicular regimes as it undergoes gravitational fragmentation into denser feather structures.

4 Results

4.1 Galactic Disc Morphology

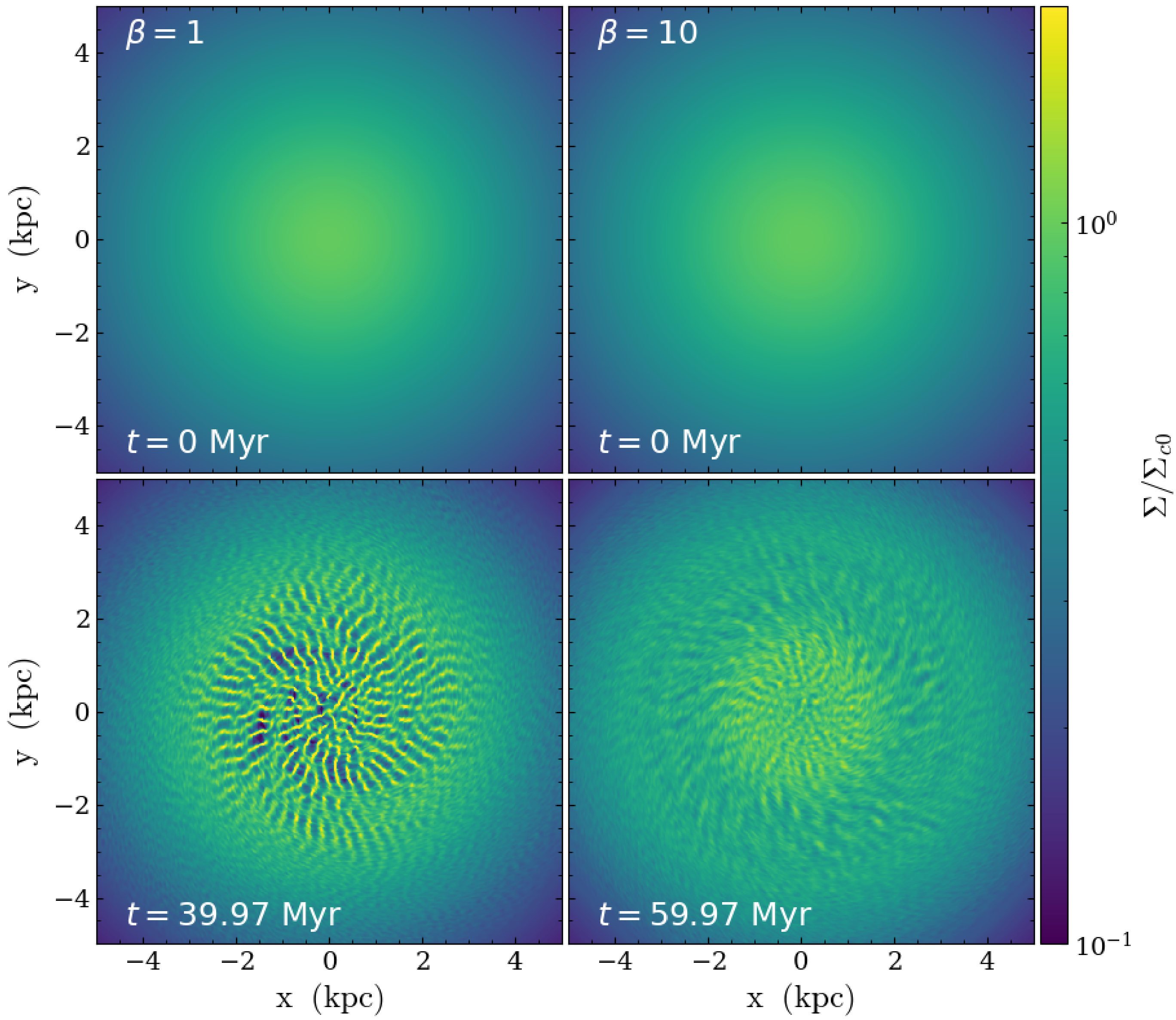

Figure 7: Face-on surface density projections of the simulated galactic disc displaying global density morphology. The top panels demonstrate the initial equilibrium states ($t = 0$ Myr) for magnetic fields at equipartition ($\beta = 1$, left) and sub-equipartition ($\beta = 10$, right) strengths. The bottom panels show the evolved states at the onset of feather formation at $t = 39.97$ Myr for $\beta = 1$ (left) and $t = 59.97$ Myr for $\beta = 10$ (right). The projected density across all panels is normalised by the initial central projected density of the galaxy (Σ/Σ_{c0}). Both simulations share identical initial conditions ($Q \approx 1$, $\mathcal{M}_c = 29$).

To analyze the global morphology of the simulated galactic disc, the 3D volume density is integrated along the vertical line of sight (z-axis) to compute the 2D projected surface density, $\Sigma = \int \rho \, dz$. Figure 7 illustrates these face-on projections. The top panels show the initial unperturbed equilibrium states at $t = 0$ Myr. The bottom panels display the evolved states at $t = 39.97$ Myr for the strongly magnetised regime ($\beta = 1$, left) and $t = 59.97$ Myr for the weakly magnetised regime ($\beta = 10$, right). These snapshots represent an evolved state of the disc, where the Toomre instability ($Q \approx 1$) has successfully initiated gravitational collapse and the feathers have emerged. Notably, the strongly magnetised disc reaches this stage earlier than the weakly magnetised one. With the feathers emerging already at $t = 39.97$ Myr for $\beta = 1$ compared to $t = 59.97$ Myr for $\beta = 10$, indicating that the presence of a dynamically significant magnetic field accelerates the fragmentation of the gas.

In the weakly magnetised regime (Figure 7, bottom right panel), the fragmentation of the gas is clearly visible. A gradual emergence of filamentary feather structures is predominantly localized within a radial distance of $R \approx 1$ to 4 kpc from the galactic center. The feathers appear highly sheared, clumping densely in the center and gradually fading outwards.

Conversely, the introduction of a dynamically strong magnetic field (Figure 7, bottom left panel) alters the spatial distribution and coherence of the gas. The filamentary feathers emerge further inward, extending from the galactic center outward to $R \approx 3$ kpc. Individual feathers appear thinner, more distinct, and geometrically more ordered, exhibiting regular spatial separation and a consistently high intensity across their entire radial extent.

Comparison between the two regimes shows that the strength of the magnetic field affects the resulting fragmentation pattern. In the strongly magnetised regime, the feathers are fewer, thinner, and more regularly spaced, while in the weakly magnetised regime they form a more fragmented and sheared pattern extending over a larger radial range. This indicates that the magnetic field influences both the onset of fragmentation and the spatial regularity of the resulting feather structures.

4.2 Magnetic Field Topology

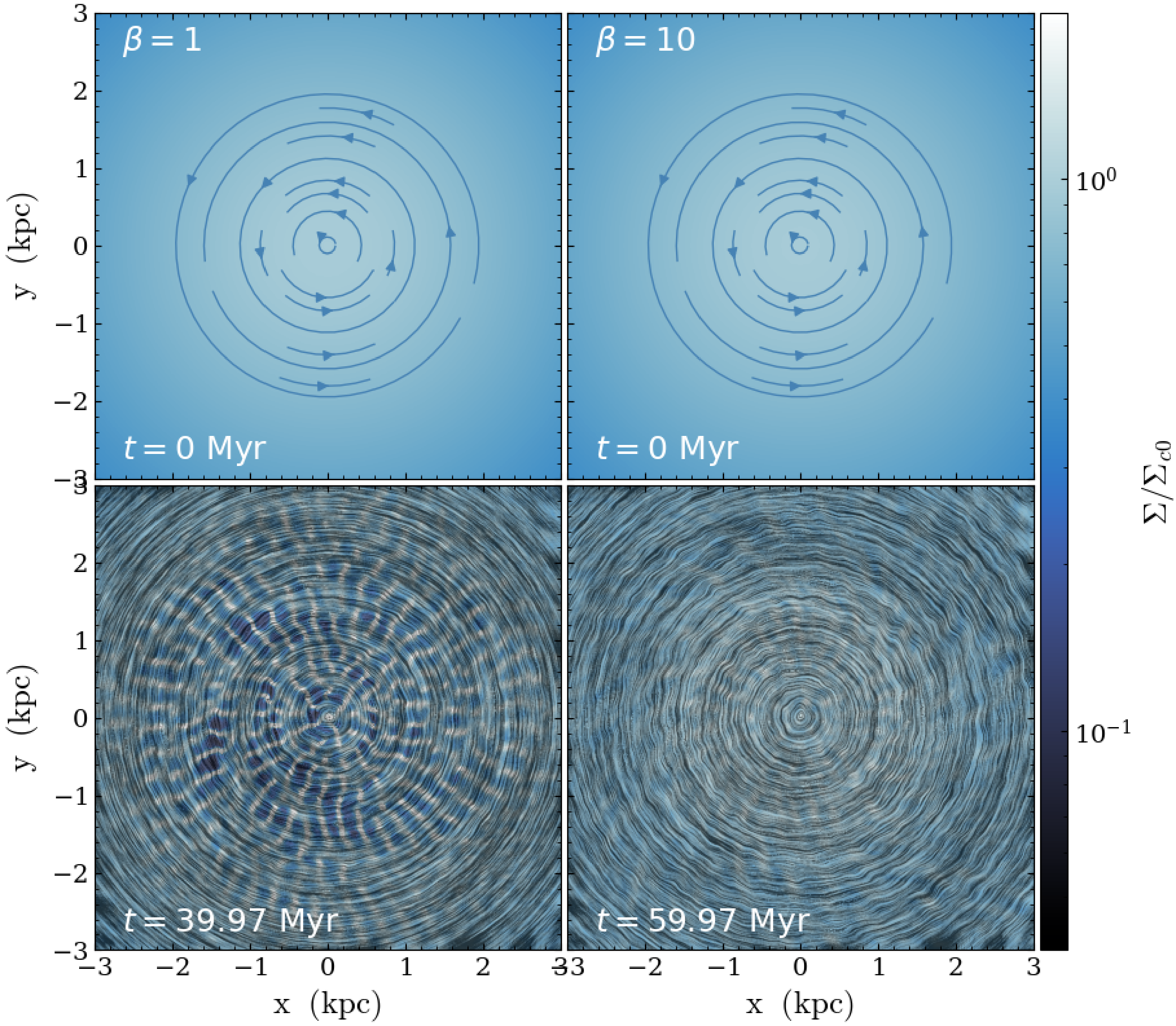

Figure 8: Evolution of the magnetic field topology of the simulated galactic disc. Surface density projections shown in Figure 7 were overlaid with magnetic field lines and visualized using Streamplot for the top panels and Line Integral Convolution (LIC) for the bottom panels. The top panels display the initial equilibrium states ($t = 0$ Myr) for magnetic fields at equipartition ($\beta = 1$, left) and sub-equipartition ($\beta = 10$, right) strengths. The bottom panels display the evolved states at the onset of feather formation ($t = 39.97$ Myr for $\beta = 1$, and $t = 59.97$ Myr for $\beta = 10$). To facilitate a direct visual comparison, the projected surface density across all panels is normalised by the initial central projected density of the galaxy (Σ/Σ_{c0}). The initially uniform, azimuthal magnetic field lines develop curved features as feathers form.

To visually analyze the topology of the magnetic fields in the plane of the disc, the in-plane magnetic field vectors were visualized using the Line Integral Convolution (LIC) method. The LIC integrates the magnetic field vectors to calculate streamline paths. It then convolves a static background image of random pixels along those paths, generating continuous streamlines that trace the flow and orientation of the magnetic fields. Figure 8 presents these magnetic field textures overlaid on the projected surface density maps for both the $\beta = 1$ and $\beta = 10$ regimes.

In the initial states (Figure 8, top panels at $t = 0$ Myr), both regimes show azimuthal symmetry, with field lines tracing circular paths around the galactic center. As the simulations evolve to the feather forming states, we can observe that for both regimes, the magnetic field lines develop curved features, which is caused by the flux freezing effect as the magnetic field is coupled to the interstellar gas. The degree of this deformation is determined by the plasma beta (β), which is defined in Section 3.1.

In the weakly magnetised environment (Figure 8, bottom right panel, $\beta = 10$), the thermal pressure dominates the magnetic pressure, resulting in significantly curved field lines as they are dragged along by the gas, with little resistance from the field itself. Conversely, for the $\beta = 1$ regime (Figure 8, bottom left panel), magnetic pressure is equivalent to the thermal pressure of the gas, so while the magnetic field is dragged by the flow, it also influences it. The overall magnetic topology appears significantly less curved and maintains a much more azimuthal structure compared to the high-β case.

4.3 Global Magnetic Alignment

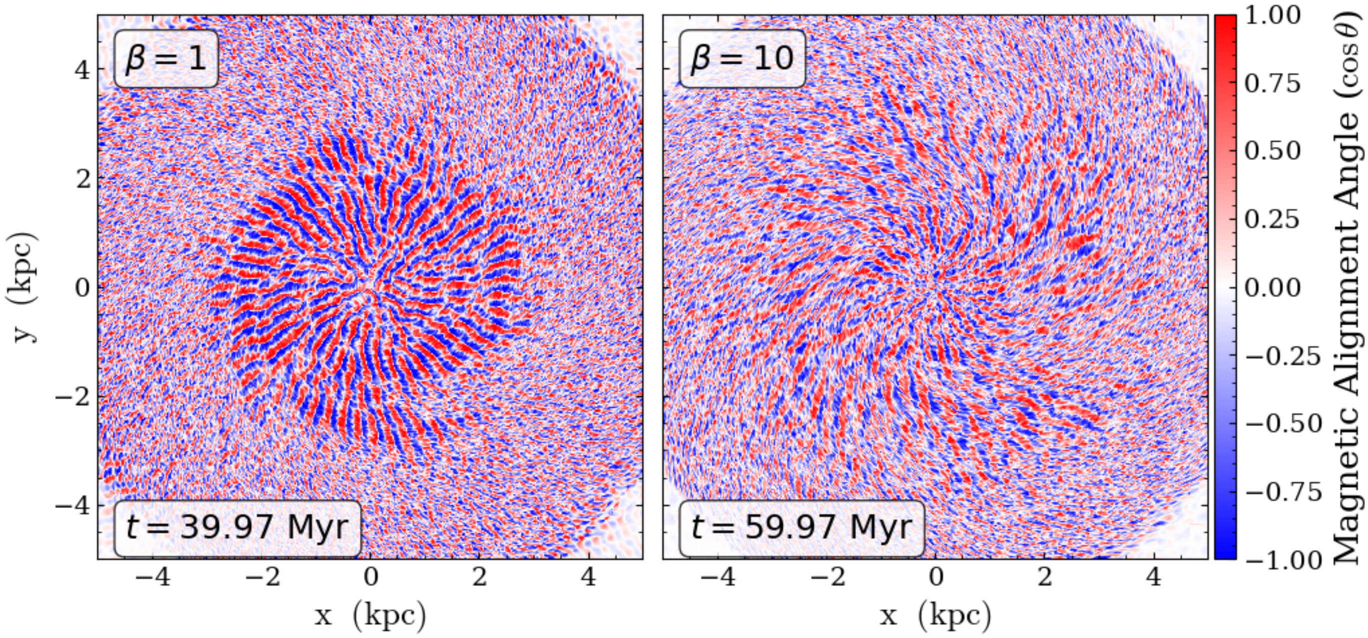

Figure 9: Spatial distribution of the relative orientation angle at $t = 39.97$ Myr for magnetic fields at equipartition ($\beta = 1$, left) and $t = 59.97$ Myr at sub-equipartition ($\beta = 10$, right) strengths. 2D maps displaying the cosine of the angle ($\cos\phi$) between the local gas density gradient ($\nabla\rho$) and the magnetic field vector ($\mathbf{B}$). Values approaching $\cos\phi = \pm 1$ (red/blue extremes) indicate regions where the density gradient is parallel or anti-parallel to the magnetic field, corresponding to gas structures that are physically perpendicular to the field lines. Values near $\cos\phi = 0$ (white/neutral) indicate density structures aligned parallel to the field. The alternating pattern of $+1$ and -1 across the dense ridges visually indicates a predominantly perpendicular structural alignment for both plots.

To quantitatively assess the physical relationship between the gas structures and the magnetic field seen in the last section, the spatial distribution of the relative orientation angle, defined as

$\cos\phi = (\nabla\rho \cdot \mathbf{B})/(|\nabla\rho||\mathbf{B}|)$, was mapped across the galactic disc. Figure 9 illustrates this alignment for both magnetisation regimes, displaying a structured, alternating pattern of $\cos\phi \approx +1$ and -1 across the dense ridges.

Looking first at the strongly magnetised regime (left panel, $t = 39.97$ Myr), we observe a sharply defined alternating pattern, particularly within the prominent structural features in the central regions of the galaxy where the feathers are most coherent and intensely defined. Physically, this pattern can be understood from the formation history of the system. As shown in Figure 7 (lower left panel), the feathers formed as predominantly radial structures, while the initial magnetic field is set up azimuthally. Because the plasma $\beta = 1$ in this regime, the magnetic pressure is sufficient to resist the gas flow, and the field lines remain mostly azimuthal, slightly curved but largely preserving their initial topology (see Figure 8, lower left panel). With the density gradient of a radial feather pointing orthogonally to its axis (in the azimuthal direction), this naturally aligns the density gradient vectors parallel and anti-parallel to the underlying magnetic field, producing the sharp alternating pattern of $+1$ and -1 seen across the dense ridges.

A similar alternating pattern is present in the weakly magnetised regime (right panel, $t = 59.97$ Myr), but it exhibits a noticeably lower contrast. In this case, the feathers remain somewhat radial in the denser regions but are highly sheared, especially towards their boundaries (see Figure 7, lower right panel). Because the plasma $\beta = 10$, the magnetic tension is not sufficient to resist the gas flow, and the field lines are dragged and deformed along with the gas (see Figure 8, lower right panel). Within the feathers, the alternating pattern is still visible, though less sharply defined than in the strongly magnetised case. At the periphery of the feathers, however, we observe regions of perpendicular alignment between the density gradients and the magnetic field, corresponding to $\cos\phi \approx 0$, which appears as the white colouring along the feather boundaries.

4.4 Variation of Alignment Parameter with Density

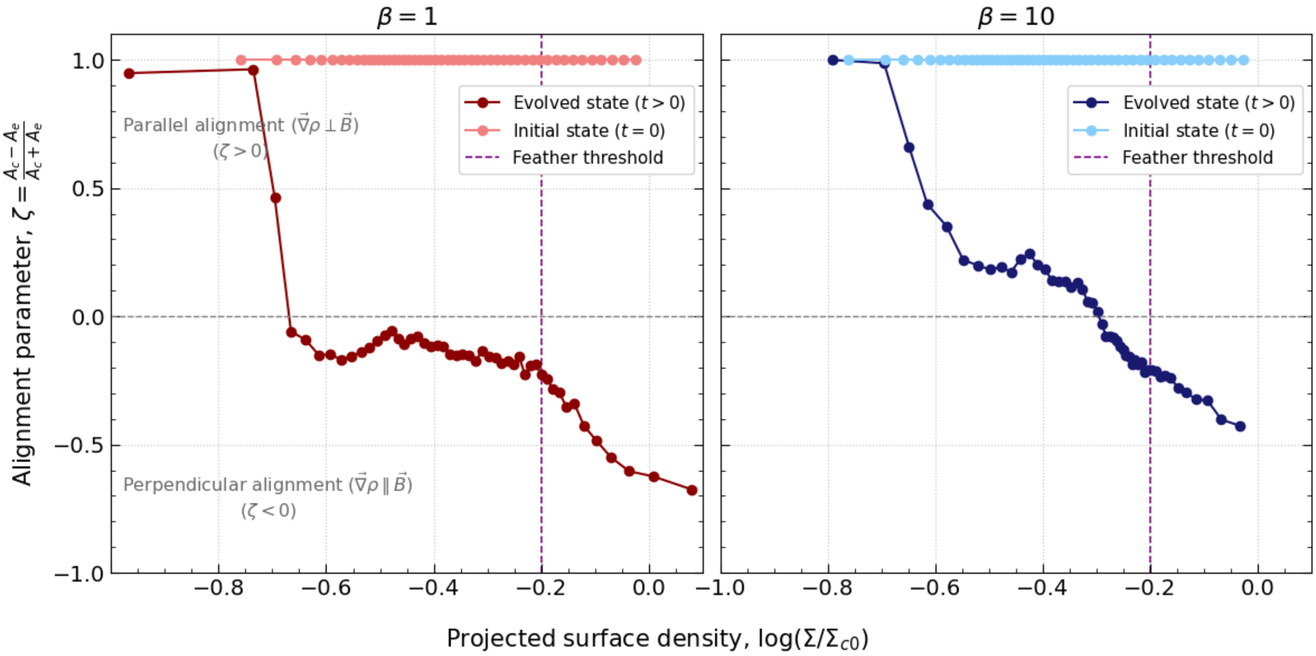

Figure 10: Density-dependent magnetic alignment of gas structures. The HRO shape parameter ζ is plotted as a function of the log-normalised projected surface density $(\log(\Sigma/\Sigma_{c0}))$. The parameter ζ quantifies the physical orientation of the gas: positive values ($\zeta > 0$) indicate structures aligned predominantly parallel to the magnetic field, while negative values ($\zeta < 0$) indicate a perpendicular alignment. The plot is divided into two panels to separate the magnetic regimes: the left panel shows the magnetic fields at equipartition strengths ($\beta = 1$) in shades of red, and the right panel shows sub-equipartition strengths ($\beta = 10$) in shades of blue. Within each panel, the evolution of the gas is tracked across two stages, with darker shades representing later times: the initial reference state ($t = 0$ Myr) and the evolved state at the onset of feather formation ($t = 59.97$ Myr for $\beta = 10$, $t = 39.97$ Myr for $\beta = 1$). The vertical purple dashed line marks the density threshold for feather formation.

The physical alignment between the gas structures and the local magnetic fields across different density thresholds is quantified in Figure 10. This figure plots the HRO shape parameter ζ as a function of the increasing normalized logarithmic surface density. As defined in Section 2.3, the ζ parameter provides a quantitative measure of this orientation, where positive values denote predominant parallel alignment and negative values denote predominant perpendicular alignment, while values close to zero yield inconclusive results.

For the initial reference states ($t = 0$ Myr) of both the strongly ($\beta = 1$) and weakly ($\beta = 10$) magnetised discs, the shape parameter remains constant at $\zeta \approx 1$ across the entire density range. Although there are no density structures present at $t = 0$, the initial setup features a radially outward density gradient. This results in concentric, ring-like density contours that are aligned with the initial magnetic field.

In the evolved states ($t = 39.97$ Myr for $\beta = 1$, and $t = 59.97$ Myr for $\beta = 10$), the structural alignment exhibits a strong density dependence. In the lower density regimes, the alignment remains parallel, with ζ values at $+1$. However, as the surface density increases, both graphs demonstrate a significant drop in ζ, indicating a transition from the parallel configuration. The zero point into the negative regime is crossed at a logarithmic density of approximately

-0.65 for the strongly magnetised ($\beta = 1$) panel and -0.3 for the weakly magnetised ($\beta = 10$) panel. Notably, for the $\beta = 10$ case the parallel alignment persists up to significantly higher densities than for $\beta = 1$, meaning that a substantial amount of lower-density gas remains predominantly parallel to the magnetic field before the transition occurs. This is consistent with the $\cos\phi$ (Figure 9, right panel), where the white $\cos\phi \approx 0$ regions along the feather peripheries correspond to these lower-density regimes and indicate the same predominantly parallel alignment between the density structures and the magnetic field.

We can see that the drop in the alignment parameter coincides with regions approaching the feather formation threshold, located at a logarithmic density of approximately -0.2. Beyond this threshold, ζ continues to decrease, and in the highest density regimes, representing the fully formed feather structures, both evolved states converge to highly negative ζ values. The strongly magnetised case reaches a substantially more negative minimum ($\zeta \approx -0.7$) compared to the weakly magnetised case ($\zeta \approx -0.45$), indicating that perpendicular alignment is more dominant when the magnetic field is dynamically significant. Finally, both evolved states demonstrate a common feature, following the initial sharp decline in ζ, a transient saturation (brief increase) occurs before it continues decreasing to more negative values.

5 Discussion

5.1 Physical Interpretation of the Magnetic Alignment

A consistent feature across both magnetic regimes is that the gas begins in a state of parallel alignment ($\zeta \approx +1$) at low densities. This is a direct consequence of the initial conditions as the magnetic field is initialized as a uniform toroidal field which is aligned with the azimuthal flow of the gas. Since the low-density gas has not yet undergone significant gravitational perturbation, its structure remains oriented along the azimuthal direction, naturally parallel to the field lines.

The two magnetic regimes show significantly different transition densities at which ζ crosses zero for the evolved states. For the strongly magnetised case $\beta = 1$, this transition occurs at notably lower densities and is comparatively sharp, while for the weakly magnetised case $\beta = 10$ it occurs later, closer to the feather formation threshold and proceeds more gradually. This contrast suggests that both the location and the sharpness of the transition may serve as a measure of the dynamical importance of the magnetic field, distinguishing regimes in which the field is dominant from those in which it is sub-dominant. This difference can be interpreted through the role of magnetic pressure in the dynamics. In the $\beta = 1$ regime, the magnetic pressure is comparable to the thermal pressure of the gas, meaning the magnetic field is dynamically significant. As a consequence of flux freezing, the field lines are coupled to the gas flow, but the magnetic tension resists stretching and deformation. This results in field lines that retain a more azimuthal topology, as shown in Figure 8, forcing density structures into perpendicular alignment at lower densities. Conversely, in the $\beta = 10$ regime, thermal pressure dominates over magnetic pressure, allowing the field lines to be more easily dragged and deformed by the gas flow. Thus, the transition to perpendicular alignment occurs at higher densities.

While our results suggest that within dense feather structures both regimes converge to predominantly perpendicular alignment ($\zeta < 0$), we caution that this behavior must be interpreted carefully. As these densest regions might not be sufficiently resolved in our simulations. Moreover, in a real galaxy, these environments would be heavily influenced by the process of star formation, which we do not include. Keeping the limitation in mind, this trend suggests that once gravitational collapse drives the gas above the feather formation threshold, the geometry of the resulting dense structures dictates the local alignment, largely independent of the magnetization. However, below this threshold, in the lower-density interarm regions, the two regimes behave differently, with the strongly magnetised case showing a more pronounced and earlier transition. This distinction may offer an observational indicator for the magnetic field strength in environments where feathers are present.

5.2 Prospects for Observational Comparison

The methodology applied in this thesis can potentially be extended to observational data of external galaxies. Borlaff et al. (2023) analyzed the magnetic field structures of nearby galaxies using far-infrared (FIR) and radio (3 and 6 cm) polarimetric observations. Their study demonstrated that FIR wavelengths trace the magnetic fields associated with dense, cold, and turbulent star-forming regions, while radio observations trace the magnetic fields in the warmer, more diffuse regions of the interstellar medium. Although both methods are derived from the polarisation of the observed radiation, they rely on different physical mechanisms, which is why they are sensitive to different phases of the gas. The FIR measurements detect the polarised thermal emission from interstellar dust grains. These elongated grains align with their short axis parallel to the local magnetic field, so that their emission is polarised perpendicular to the field, and the plane-of-sky field orientation is recovered by rotating the measured polarisation angle by $90°$. Because interstellar dust is concentrated in the cold, dense gas, this method is most sensitive to the magnetic field in the star-forming regions. The radio measurements instead detect the linearly polarised synchrotron emission produced by relativistic cosmic-ray electrons spiraling around the magnetic field lines. The polarisation plane of this emission is also oriented perpendicular to the field component in the plane of the sky, so the field orientation is recovered from the polarisation angle in the same way, after correcting for the Faraday rotation introduced along the line of sight. Because the synchrotron-emitting electrons fill the warm, diffuse gas, this method instead probes the magnetic field in the more extended regions of the disc.

The HRO algorithm utilized in this thesis could be applied to this observational data to investigate the physical alignment of gas structures. For this purpose, the radio observational data would be the most appropriate fit for the ideal MHD simulations analyzed here. Borlaff et al. (2023) noted that the magnetic fields traced at radio wavelengths are larger in scale and more ordered. Because it traces the diffuse gas, the radio magnetic field morphology is primarily dictated by galaxy-wide mechanisms, such as global gravitational interactions and differential rotation. These are exactly the large-scale mechanisms that are active in the simulations analyzed in this work. Therefore, applying the HRO algorithm to the radio wavelength data would allow for a direct comparison between the simulated environments and the observed diffuse interstellar medium.

Conversely, applying this methodology to the FIR observational data would be problematic at the moment due to the current limitations of the simulation runs. The FIR data is highly sensitive to the localized dynamics of star-forming processes. The simulations analyzed in this study utilize a simplified, idealized framework that does not include active star-forming regions or supernovae. Therefore, a direct comparison to the cold, dense gas phase observed in FIR would not be accurate. Future improvements to the simulation framework would need to incorporate these stellar feedback mechanisms before the magnetic alignment can be evaluated.

6 Outlook

This thesis investigated the role of magnetic fields in the formation of feather structures in spiral galaxies by analysing isolated, self-gravitating, isothermal magnetohydrodynamic simulations at two different magnetisation levels. The HRO technique was applied to quantify the alignment between gas density structures and the local magnetic field as a function of log-normalised projected surface density. The main finding is that the density at which the alignment transitions from parallel to perpendicular depends on the dynamical importance of the magnetic field. In the strongly magnetised regime ($\beta = 1$), the transition occurs at lower densities, while in the weakly magnetised regime ($\beta = 10$) it occurs at densities roughly a factor of two higher, close to the feather formation threshold itself. Beyond this threshold, both regimes converge to predominantly perpendicular alignment, although the strongly magnetised case reaches more negative values of the alignment parameter ζ. This suggests that the location and sharpness of the transition may serve as a diagnostic of the magnetic field strength in galactic discs.

Several directions for future work follow from these results. In this thesis we only considered two values of the plasma β, and extending the analysis to a broader range of magnetisation levels would clarify how the transition density and the depth of alignment scale with the dynamical importance of the magnetic field. Another possible improvement concerns the physics included in the simulations. The current simulations are idealised and do not include stellar feedback, supernova explosions, or active star formation. Including these processes in future simulations would allow the alignment analysis to be extended into the dense, star-forming regime, where the current results are limited.

Finally, the methodology developed in this thesis could potentially be extended to the observational data. As discussed in Section 5.2, the Histogram of Relative Orientations could be applied to polarimetric data of nearby galaxies, with radio observations providing the most appropriate comparison to the diffuse, large-scale magnetic fields traced in the present simulations. A direct application to the data of Borlaff et al. (2023) would allow the simulated alignment behaviour to be tested against observed magnetic field structures in real spiral galaxies.

References

Arora, R., Federrath, C., Krumholz, M., & Banerjee, R. (2025). Formation of filaments and feathers in disc galaxies: Is self-gravity enough? *arXiv preprint arXiv:2502.18565*.

Beck, R. (2016). Magnetic fields in spiral galaxies. *The Astronomy and Astrophysics Review*, 24(1), 4.

Borlaff, A. S., Lopez-Rodriguez, E., Beck, R., Clark, S. E., Ntormousi, E., Tassis, K., et al. (2023). Extragalactic Magnetism with SOFIA (SALSA Legacy Program). V. First Results on the Magnetic Field Orientation of Galaxies. *The Astrophysical Journal*, 952(4), 24.

Cai, K., Huang, B., Girart, J. M., Stephens, I. W., Sánchez-Monge, Á., Le Gouellec, V. J. M., Jiao, W., He, Q., Lu, Z.-J., & Liang, E. (2026). B-field Orion Protostellar Survey (BOPS). IV: The Relative Orientation Between Magnetic Fields and Density Structures in Young Protostellar Envelopes. *arXiv preprint arXiv:2602.05316*.

Choudhuri, A. R. (1998). *The Physics of Fluids and Plasmas: An Introduction for Astrophysicists*. Cambridge University Press.

Ferrière, K. (2020). Plasma turbulence in the interstellar medium. *Plasma Physics and Controlled Fusion*, 62(1), 014014.

Han, J. L. (2017). Observing Interstellar and Intergalactic Magnetic Fields. *Annual Review of Astronomy and Astrophysics*, 55, 111–157.

Konstantinou, A., Ntormousi, E., & Tassis, K. (2026). What does it mean to take the mean? The effect of the averaging scale on the characterization of interstellar turbulence. *arXiv preprint arXiv:2602.15932*.

Kim, W.-T., Kim, C.-G., & Ostriker, E. C. (2020). Local Simulations of Spiral Galaxies with the TIGRESS Framework. I. Star Formation and Arm Spurs/Feathers. *The Astrophysical Journal*, 898, 35.

Körtgen, B., Banerjee, R., Pudritz, R. E., & Schmidt, W. (2019). Global dynamics of the interstellar medium in magnetized disc galaxies. *Monthly Notices of the Royal Astronomical Society*, 489(4), 5004–5021.

Körtgen, B., & Soler, J. D. (2020). The relative orientation between the magnetic field and gas density structures in non-gravitating turbulent media. *Monthly Notices of the Royal Astronomical Society*, 499(4), 4730–4739.

La Vigne, M. A., Vogel, S. N., & Ostriker, E. C. (2006). An HST Archival Survey of Feathers in Spiral Galaxies. *arXiv preprint astro-ph/0606761*.

Meidt, S. E., Rosolowsky, E., Sun, J., et al. (2023). PHANGS-JWST First Results: ISM structure on the turbulent Jeans scale in four disk galaxies observed by JWST and ALMA. *The Astrophysical Journal Letters*, 944, L18.

Soler, J. D., Hennebelle, P., Martin, P. G., Miville-Deschênes, M.-A., Netterfield, C. B., & Fissel, L. M. (2013). An Imprint of Molecular Cloud Magnetization in the Morphology of the Dust Polarized Emission. *The Astrophysical Journal*, 774(2), 128.

Soler, J. D., & Hennebelle, P. (2017). What are we learning from the relative orientation between density structures and the magnetic field in molecular clouds? *arXiv preprint arXiv:1705.00477*.

Shukurov, A., & Subramanian, K. (2021). *Astrophysical Magnetic Fields: From Galaxies to the Early Universe*. Cambridge University Press.

Toomre, A. (1964). On the gravitational stability of a disk of stars. *The Astrophysical Journal*, 139, 1217–1238.